G. Panzarasa, S. Aghion, G. Soliveri, G. Consolati, R. Ferragut
*Positron Annihilation Spectroscopy: a New Frontier for Understanding Nanoparticle Loaded Polymer Brushes*
Nanotechnology, Vol. 27, N. 2, 2016, 02LT03 (8 pages)
doi:10.1088/0957-4484/27/2/02LT03

# Positron annihilation spectroscopy: a new frontier for understanding nanoparticle-loaded polymer brushes

Guido Panzarasa[1,6], Stefano Aghion[2,3,6], Guido Soliveri[4], Giovanni Consolati[5] and Rafael Ferragut[2,3]

1 Department of Science and Technological Innovation, Università del Piemonte Orientale 'Amedeo Avogadro', viale T. Michel 11, 15100 Alessandria, Italy
2 LNESS, Department of Physics, Politecnico di Milano, via Anzani 42, 22100 Como, Italy
3 Istituto Nazionale di Fisica Nucleare, via Celoria 16, 20133 Milano, Italy
4 Department of Chemistry, Università degli Studi di Milano, via C. Golgi 19, 20133 Milano, Italy
5 Department of Aerospace Science and Technology, Politecnico di Milano, via La Masa 34, 20156 Milano, Italy
6 These authors contributed equally.

## Abstract

Nanoparticle-loaded polymer brushes are powerful tools for the development of innovative devices. However, their characterization is challenging and arrays of different techniques are typically required to gain sufficient insight. Here we demonstrate for the first time the suitability of positron annihilation spectroscopy (PAS) to investigate, with unprecedented detail and without making the least damage to samples, the physico-chemical changes experienced by pH-responsive polymer brushes after protonation and after loading of silver nanoparticles. One of the most important findings is the depth profiling of silver nanoparticles inside the brushes. These results open up a completely new way to understand the structure and behavior of such complex systems.

## Introduction

Polymer brushes are at the cutting edge of modern polymer science, thanks not only to their unique properties but also to the problems posed by their characterization. A polymer brush is defined as an assembly of polymer chains anchored by one end to a surface, with a coverage sufficiently high that the chains are forced to stretch away from the surface to avoid crowding. The analysis of these structures is challenging: because of their reduced dimensionality, assumptions based on analogous solution or bulk systems do not necessarily hold. For this reason there is a strong desire to understand their fundamental properties at interfaces and in developing new applications [1, 2]. The basic physics of polymer brushes was established three decades ago and notable progress has been made since.

However, one of the less understood and still challenging problems in polymer science and technology is the behavior of hybrid systems made of polymer brushes and nanoparticles. Both theoretical [3–8] and experimental [9–11] studies were stimulated not only by the variety of useful applications for the resulting nanocomposites [12] but also because understanding their behavior is of paramount importance in many different domains ranging from biology to organic electronics. In biology and related disciplines, being able to predict the behavior of polymer layers with nanoscale objects like proteins means the possibility of

designing efficient antimicrobial, antifouling, blood- and tissue-compatible surfaces [13–17]. Applications in drug delivery [18] and microfluidics [19] are promising as well. In organic electronics, photovoltaic devices exploiting the interaction of quantum dots with donor-acceptor brushes has already been demonstrated [20], but still the conditions governing nanoparticle distribution are unknown. The development of novel optical sensors [21, 22] and actuators [23] will also benefit from plasmonic noble metal nanoparticles embedded in stimuli-responsive (e.g. pH- and thermo-responsive) brushes.

Whereas theoretical studies are gaining momentum thanks in particular to progress in computer simulations, the lack of techniques allowing physical observation of such complex systems is a great hindrance to significant progress in the development of brush-nanoparticle composites. Taking a glimpse of the real system would be the ultimate way to know the actual properties of a composite. It is already difficult to properly characterize nanometer-sized polymer layers such as polymer brushes and the problems posed by nanoparticle-loaded polymer brushes are especially tough. Despite several groups investigating the formation of nanoparticles inside or on top of polymer brushes, only a few experimental studies are available on nanoparticle infiltration into polymer brushes. To determine the distribution of nanoparticles inside the brushes is of paramount importance; however, direct visualization of polymer brush-embedded nanoparticles is possible only by transmission electron microscopy on cut samples. The special skills required and the occurrence of artifacts due to incorrect sample preparation along with its intrinsically destructive nature make this approach impractical. For this reason, the vast majority of the studies relied on the use of indirect techniques such as ellipsometry [24], x-ray reflectivity [25] and UV–vis spectroscopy [26, 27].

The introduction of a one-step, non-invasive technique that allows probing of the distribution of nanoparticles in polymer brushes would act as a true game-changer for this field of applied research. We report here for the first time the use of positron annihilation spectroscopy (PAS) as a powerful means to investigate nanoparticle loading into stimuli-responsive polymer brushes.

In the PAS technique positrons, positively charged antiparticles of electrons, are implanted with a controlled kinetic energy into the studied material and annihilate either as free positrons with the electrons in two 511 keV gamma-rays or in the form of a positron–electron bonded state called positronium. Positronium (Ps) is the lightest element, about $10^{-3}$ times lighter than hydrogen, and exists in the ground state in two sublevels: singlet (para-Ps, p-Ps) and triplet (ortho-Ps, o-Ps), according to the spins of the electron and positron (antiparallel or parallel, respectively) (scheme S2). In vacuum, their lifetimes are very different, 0.125 and 142 ns for p-Ps and o-Ps, respectively. Also annihilation features in vacuum are different: p-Ps annihilates with the emission of two γ-rays (511 keV each), while o-Ps annihilates by emitting three γ-rays, producing a continuous energy distribution for each photon between 0 and 511 keV, where the energy sum of the three photons of the o-Ps annihilation is 1022 keV. When o-Ps is formed inside a cavity of a material (such as a free volume hole in a polymer, a cage in a zeolite, a pore in a porous medium), the three-γ annihilation probability is reduced by the pick-off effect, that is, the positron of the o-Ps may annihilate with an electron of the cavity surface in a relative singlet state with emission of two γ-rays instead of three.

Under the collective name of PAS an array of techniques are grouped that have been developed to probe atomic/molecular defects and interfacial properties in materials, with applications ranging from metallurgy [28] to soft matter [29–31]. As has been demonstrated, Ps forms into the free volumes of many polymers and PAS can detect buried, isolated pores of 0.2–50 nm size, which are not accessible to conventional probes. Therefore the study of free volumes in polymers [32] and of transport mechanisms in membranes [28–33] is enabled, in a completely non-invasive way, by monitoring the annihilation of positronium. In the field of polymer research, the most frequent PAS techniques are [34]: (i) positron annihilation lifetime spectroscopy (PALS) which measures the positron lifetime implanted in a sample material and (ii) Doppler broadening of annihilation radiation which measures the broadening of the 511 keV peak coming from the

positron–electron annihilations. When the size of the open spaces is at the nanometer scale (>1 nm) and ortho-Ps annihilation in three gamma-rays can be observed [35, 36], another PAS technique known as the '3γ-method' is also useful [37, 38].

In recent years PAS with a variable-energy positron beam has emerged as a powerful technique for the characterization of thin films [39, 40], allowing depth-profiles from tens of nanometers up to several micrometers. To carry out PAS measurements on thin films it is necessary to tune the positron implantation energy in order to conduct a depth-profile study. The LNESS facility in Como is equipped with an electrostatic slow energy positron beam (by this point onwards referred to as the VEPAS beam), whose energies range from 0.1 keV to 20 keV, coupled with two hyperpure Ge detectors. In the VEPAS beam (refer to the supplementary data for details, pp S15–S16) positrons are emitted from a 10 mCi radioactive $^{22}$Na source and they are subsequently moderated by means of a W thin monocrystalline film (1 μm thick, [100] oriented). Since the $^{22}$Na positron energy distribution is very spread with a maximum at about 0.54 MeV, in order to tune the energy of the beam a W micrometric foil which re-emits positrons at ~2.5 eV with an efficiency of $10^{-3}$–$10^{-4}$ is employed. The moderated positrons are then accelerated and implanted into the samples at a tunable kinetic energy. Once implanted positrons penetrate to a depth which depends on their initial kinetic energy they then thermalize, i.e. slow down, on a timescale of picoseconds. Afterwards the positrons diffuse and, as described above, can annihilate as free positrons or as positronium.

The key motivation of the present study is to demonstrate that positron annihilation spectroscopy is the only actual technique allowing the study of nanoparticle distribution in polymer brushes with a single analysis and without damaging the sample. A system made of silver nanoparticles (AgNPs) embedded in grafted-from poly(dimethylaminoethyl methacrylate) (PDMAEMA) brushes obtained by surface-initiated atom transfer radical polymerization (SI-ATRP) was chosen as a representative case study for plasmonic nanoparticle-loaded stimuli-responsive polymer brushes, a system with promising applications, especially in the development of sensors [41, 42].

## Methods

*Polymer brushes by surface-initiated polymerization and their loading with silver nanoparticles.*

The use of a controlled radical polymerization technique like SI-ATRP allowed us to obtain brushes with different thicknesses simply by varying the polymerization time (figure S1). According to previous studies [43], the grafting density σ of the chains is expected to be at least 0.4 chains nm$^{-2}$. The distance between two adjacent grafted end-groups can be estimated as $g = \frac{1}{\sqrt{\sigma}} \approx 1.6$ nm and compared to the characteristic size of the chains in order to evaluate their conformation. As the polymer layer is in a dry state, we assumed that the grafted chains adopt a collapsed state with a characteristic dimension $G \approx aN^{0.33}$ where $a$ is a characteristic dimension of the repeating unit (0.25 nm for methacrylates) and $N$ is the average number of repeating units (i.e. the molecular mass) of the polymer chains which has been estimated by XRR results (figure 1(b), figure S2 and table S1). The brush conformation prevails at high grafting density or $g \ll G$ a condition our estimates suggest to be fulfilled for the investigated samples ($G$ > 8 nm) which can then be considered as polymer brushes.

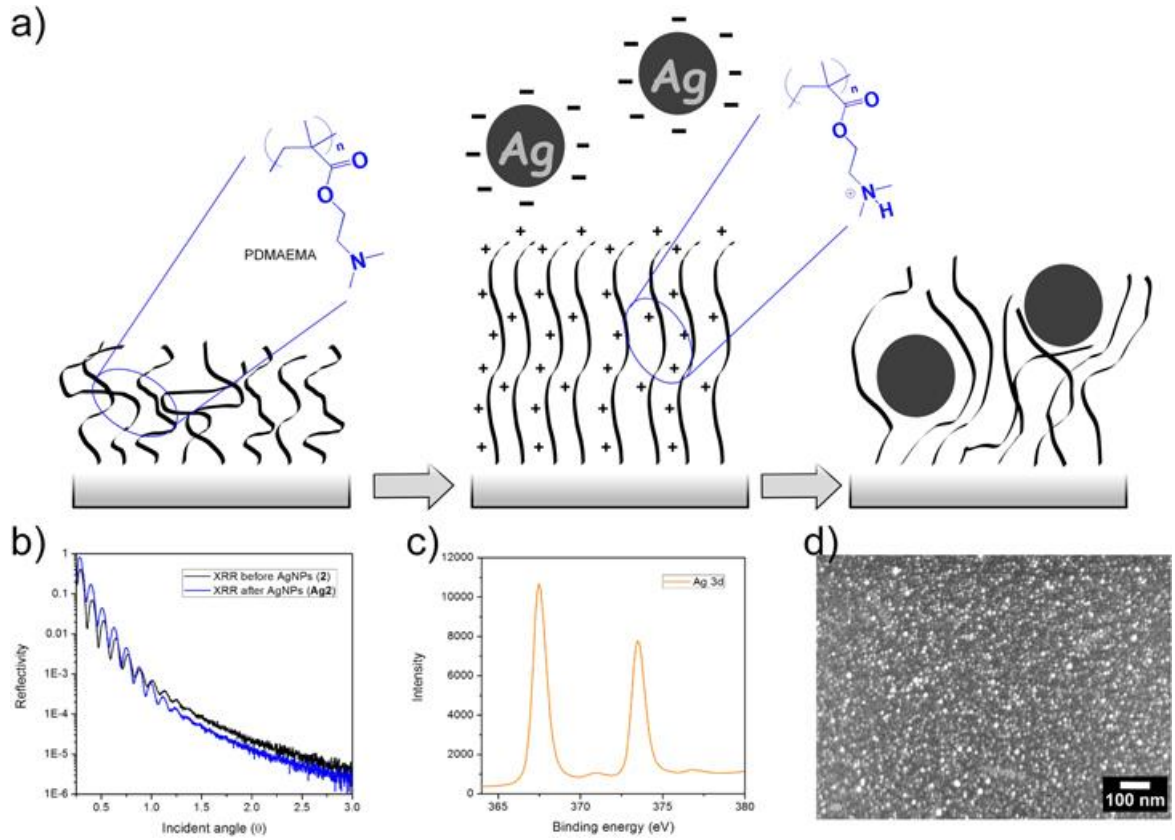


**Figure 1**. (a) Schematic representation of the PDMAEMA brushes before and after protonation and the uptake of silver nanoparticles. (b) Representative XRR spectra of a brush before and after incorporation of AgNPs. (c) XPS signals of Ag 3d from brush-embedded nanoparticles. (d) Representative SEM image of a brush-nanoparticle composite.

PDMAEMA is a weak polyelectrolyte with pKa ~ 7, which makes its tertiary amine group easily protonated and deprotonated by immersion in acid or basic solutions, respectively [44]. Protonation induces the formation of positive electrostatic charges and this effect, combined with excluded volume interactions and the osmotic pressure due to counterions, causes the chains to repel each other and swell after water absorption. For this reason, pH variations are accompanied by changes in the brushes hydrophilicity that can be easily followed by water contact angle ($\vartheta_w$) measurement: the original $\vartheta_w$ 55° changed to 40° after immersion in 0.1 M $HNO_3$ but it was restored by immersion in 0.1 M NaOH. This process could be repeated indefinitely. The positive charges on protonated PDMAEMA brushes facilitate the incorporation of pre-made, negatively charged, silver nanoparticles [45, 46] with a simple immersion step. The incorporation of silver nanoparticles into the brushes was found to induce great morphological changes in the latter. The surface of as-prepared PDMAEMA brushes appeared to be homogeneous and smooth (figure S3) but became rough after being dipped in the suspension of AgNPs (figure 1(d)). From scanning electron microscopy images, silver nanoparticles are identifiable as spherical shapes protruding from the surface of the brushes. Backscattered electrons (figure S4) were used to check for the presence of free nanoparticles on top of the brushes but the particles were buried in the polymer film, which appears reasonable considering that the mean thickness of the brushes was at least double with respect to the mean diameter of AgNPs (~10 nm).

Due to the relevant optical applications described for noble metal particle–polymer brush nanocomposites, the UV-visible absorption spectra for the AgNPs-PDMAEMA brushes were acquired for samples grown on transparent glass substrates, revealing a strong absorption band attributable to the surface plasmon resonance (SPR) of the embedded silver nanoparticles (see the supplementary data, figure S5).

X-ray photoelectron spectroscopy (XPS) was used to investigate each synthetic step (for details refer to the supplementary data, figure S6) and to demonstrate the effective incorporation of silver nanoparticles.

Despite that in the AgNP-loaded brushes the N 1 s signal was confused by the strong Ag 3d peak, precious information about the chemical environment of the nanoparticle surface could be obtained (figure 1(c)). It is noteworthy to highlight that the Ag 3d peak at 367 eV is typical of $Ag^0$, because the Ag peaks for pristine AgNPs showed a dramatic shift indicative of a strong coordination, of the type $(O=C\text{-}O)^- Ag^+$, between adsorbed citrate anions and surface silver atoms (figure S5(d)). After incorporation into the brushes the negatively charged citrate molecules neutralized with positively charged protonated PDMAEMA brushes.

Polymer brushes before and after the uptake of AgNPs were also investigated with x-ray reflectivity, which allowed one to determine their thickness and density. However, XRR was unable to confirm the presence of silver nanoparticles inside the brushes. Due to the homogeneous distribution of silver nanoparticles in the polymer matrix the fitted density values were clearly underestimated (table S2). This was due to the less definite character of the layers, as could be seen from the quenching of the Kiessig fringes at low angles.

*Positron annihilation spectroscopy*

Positron annihilation spectroscopy (PAS) measurements were performed on five samples of PDMAEMA brushes grafted from silicon substrates (n-type, 3–6 Ω $cm^{-1}$). All the relevant experimental details for their synthesis and characterization can be found in the supplementary data (pp S2–S5). Table 1 summarizes the principal characteristics of the samples. Protonation of the brushes and uptake of silver nanoparticles were investigated. The first sample listed in table 1 (PDMAEMA), representative of the as-prepared brushes, is composed of a thin layer of polymer grafted from the silicon substrate. The second sample (H+) was protonated by immersion in dilute nitric acid. The other three samples i.e. Ag1, Ag2 and Ag3 have increasing thicknesses. They were protonated and then immersed in an aqueous suspension of silver nanoparticles to allow the uptake of the latter.

| Sample | Protonation | AgNPs | Thickness (nm) |
|---|---|---|---|
| PDMAEMA | No | No | 18 ± 1 |
| H+ | Yes | No | 20 ± 1 |
| Ag1 | Yes | Yes | 27 ± 1 |
| Ag2 | Yes | Yes | 40 ± 1 |
| Ag3 | Yes | Yes | 66 ± 1 |

Table 1. Samples studied by means of PAS.

PAS measurements were conducted by means of the VEPAS beam. Thirty-eight values for the positron implantation energy were chosen between 0.1 keV and 18 keV and, for each energy value, two hyperpure Ge detectors coupled with a MCA system recorded the annihilation spectrum. The positron annihilation peak is centered at 511 keV. Its broadening is a consequence of the Doppler effect due to the electron–positron center of mass momentum with respect to the laboratory frame of reference. The *S*-parameter is then defined as the ratio between the area in the central part of the annihilation peak, within the energy range of 511 ± 0.85 keV ($p_L \leq$ 0.456 atomic units). The W-parameter ('wing' or core annihilation parameter) is taken in the high-momentum region far from the center part of the peak, within the range from 511 ± 1.8 keV to 511 ± 4 keV. The total area of the peak is taken in the range 511 ± 4.25 keV.

For each implantation energy the *S*-parameter and the three-gamma fraction F3γ were measured and are shown in figure 2. The values obtained for the W-parameter are discussed in the supplementary data (pp S17–S19). The S-parameter corresponds to the annihilation of the positrons with the valence electrons of the material, p-Ps annihilation or the o-Ps atoms undergoing a pick-off annihilation. The three-gamma fraction $F_{3\gamma}$ is calculated according to the '3γ method'. When the studied material contains big cavities (>1 nm), the annihilation of o-Ps in three gamma-rays is observed and in this case $F_{3\gamma}$ is proportional to the Ps yield. The energy distribution of each of the three gamma-rays is continuous between 0 and 511 keV. By defining $R(E)$, $E$ being the positron implantation energy, as:

$$R(E) = \frac{V}{P}$$

where *P* are the integrated counts in the peak area, within the energy region 511 ± 4.25 keV, and V is the valley area above the Compton edge, from 350 keV up to 500 keV, the three-gamma fraction $F_{3\gamma}$ is given by:

$$F_{3\gamma} = \left[1 + \frac{P_1}{P_o}\left(\frac{R_1 - R(E)}{R(E) - R_0}\right)\right]^{-1}$$

where the subscripts 0 and 1 refer to the cases with 0% and 100% Ps production, respectively.

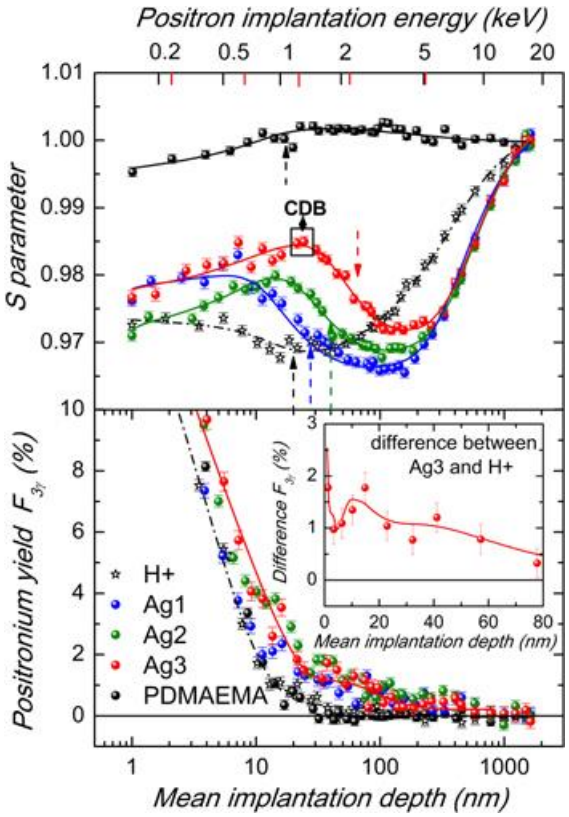


**Figure 2.** Upper panel: normalized S-parameter as a function of the positron mean implantation depth for various samples of PDMAEMA brushes on silicon substrates: as-made (PDMAEMA), after protonation (H+) and after loading of silver nanoparticles (Ag1, Ag2, Ag3). The lines through the experimental data represent the results of a best-fit procedure obtained with VEPFIT. The black and red colored ticks correspond to the average of the samples without and with silver respectively (see the supplementary data for details). Lower panel: positronium fraction profile in the studied samples. The insertion shows the difference between the F3γ for Ag3 and H+ samples (the data points are the average of two adjacent data points).

## Results and discussion

Figure 2 shows the *S*-parameter normalized to the value of this parameter in silicon ($S = S_m/S_{Si}$, where $S_{Si} \approx 0.543$ and $S_m$ is the measured value) and the three-gamma fraction $F_{3\gamma}$ as well (lower panel), for the samples listed in table 1. The data points are the average of the data obtained by the two Ge detectors. The *S* and $F_{3\gamma}$ parameters are represented as a function of the mean positron implantation depth (lower abscissa) and of the positron implantation energy (upper abscissa, black and red ticks correspond to the samples without and with Ag nanoparticles respectively). The mean implantation depths were evaluated by adopting the Makhov profiles as the stopping profiles of the implanted positrons (see the supplementary data, pp S19–S21). The dashed arrows indicate the positron implantation depths corresponding to the different brush thicknesses. It is possible to consider them as thresholds beyond which the positrons

annihilate within the interface and the silicon substrate. The continuous lines through the data points in the upper panel represent the best fits obtained with the VEPFIT program [47]. This software is a best-fit procedure based on the solution of the diffusion equation in each layer of a heterostructure, taking into account the energy dependent positron implantation profiles. The model free parameters, for each layer, are the following: the *S*-parameter value, the positron diffusion length, the electric field (when present) and the layer density.

By comparing the data shown for the PDMAEMA and H+ samples in figure 2 it is possible to observe that protonation causes a dramatic change of the S-parameter value for the brush layer. For the PDMAEMA (non-protonated) sample the implanted positrons form positronium atoms that remain confined into the free volumes (sub-nanometric cavities ~0.3 nm) [48–50], annihilating by pick-off and giving the maximum *S*-parameter value of the distributions ($S > 1$). The profile of the *S*-parameter after protonation (sample H+) drops with respect to the non-protonated sample (PDMAEMA), a fact that demonstrates the inhibition of Ps formation. This effect is a consequence of the positron traps for the H+ sample being of a different nature with respect to the non-protonated samples. By the acid-base reaction of nitric acid with the PDMAEMA tertiary amine groups, i.e. the protonation step, electric dipoles are formed along each polymer chain with the positive charges located on the protons and the negative ones on the polarized nitrogen atoms of PDMAEMA chains, which in turn attract the positrons.

The $F_{3\gamma}$ parameter profiles (lower panel in figure 2) show a practically identical behavior of the samples before and after protonation (PDMAEMA and H+, respectively). It is known that all materials form Ps at the surface (between 16 and 18% at the minimum positron implantation energy in the studied materials, see figure S8) and low $F_{3\gamma}$ values, almost zero, inside the brushes are symptomatic of only two-gamma annihilation events (free, para-Ps and ortho-Ps by pick-off annihilation without three-gamma photons).

The effect of the uptake of Ag nanoparticles in brushes with different thicknesses (27, 40 and 66 nm) is shown in figure 2. The distribution for each sample (Ag1, Ag2 and Ag3) shows a bump with a maximum centered near to the half-value of the thickness. These results clearly indicate the successful loading of AgNPs into the brushes. The changes in the S-parameter can be attributed to modifications in the chemistry of the annihilation sites or to the occurrence of cavities able to form positronium (para-Ps and pick-off–annihilated ortho-Ps). Since the tails of the two-gamma peak at a high Doppler shift come from annihilation with inner atomic shells, their study allows one to understand the nature of microstructural changes generated by the loading of AgNPs. The high-momentum region is more sensitive than the *S*-parameter to the average chemical composition in the annihilation region, i.e. it is possible to obtain a fingerprint of the chemical environment where the positrons annihilate. However, the low counting rate in the high-momentum region requires background suppression by adopting the coincidence Doppler broadening technique (CDB), i.e. to take both annihilation gammas in coincidence. CDB spectra with about $2 \times 10^7$ total counts were measured with a peak/background ratio of $10^5$ to $10^6$. The momentum resolution (FWHM) was $3.6 \times 10^{-3}$ m0 c. The experimental procedure used in this study is similar to those described in [51].

CDB measurements were performed in sample Ag3 at the maximum of the *S*-parameter bump (see the black square in figure 3, positron implantation energy 1.4 keV corresponding to a mean depth of 28 nm). Another CDB measure was performed for the H+ sample at 1 keV (near to the minimum value of the *S*-parameter). The lower panel of figure 3 shows the momentum distributions ρ of the electron–positron pairs during annihilation (related mainly to the electron velocity distribution) that contains information about the atomic orbitals from the atoms of the annihilation environment. For comparison a CDB measurement of a high purity silver bulk sample (99.999% Ag) is included. The upper panel of figure 3 shows the relative difference of the momentum distributions $(\rho - \rho H+)/\rho H+$ of the thin brush film Ag3 and the Ag bulk sample with respect to the protonated brushes H+. This representation enhances the distribution at high momentum where the chemical fingerprint of the annihilation sites is present. The bulk Ag distribution shows a remarkable difference with respect to the H+ brushes (line through zero). The

distribution of the relative difference of Ag bulk (upper panel) was divided by ten in order to make possible a comparison with the Ag3 distribution on the same scale. The Ag distribution presents peaks at ±1.8 atomic units of momentum (~ ±13 × $10^{-3}$ m0 c) that correspond to the 4d-orbitals of Ag [52, 53]. The distribution of the relative difference of sample Ag3 (red points in figure 3) shows a central narrow peak and two lateral bumps. The maximum of the lateral peaks is in good agreement with the position of the 4d-orbitals of Ag but is about 40 times less intense. The results indicate that the S-parameter would have been decreased if positrons had annihilated in Ag. However, an enhancement is observed: the reason is the central narrow peak that appears for Ag3 which, according to our interpretation, is due to the o-Ps pick-off annihilation, p-Ps annihilation and to positron annihilation in defects associated to the nanoparticle surface. These facts indicate that positrons do not actually annihilate inside the AgNPs of only 10 nm in diameter (this dimension is one order of magnitude lower than the typical positron diffusion length in Ag). Positrons are trapped at the nanoparticle surface defects and mainly form positronium into the cavities formed by the polymer chains wrapped around the nanoparticles. In the supplementary data (see pp S17–S19) results of the W-parameter supporting this interpretation are available. This explanation is coherent with F3γ results show in figure 2 (lower panel): the insert shows the difference between the distribution of the AgNPs-loaded brushes (Ag3 sample) and of the protonated brushes H+. The samples infiltrated with nanoparticles show an increase of three-gamma annihilation (1–1.5% in Ag3, see inset of figure 2) which can only be explained by the presence of open spaces with a mean diameter > ~1 nm [35, 36]. Thus, the presence of nanoparticles in the brushes are associated with the formation of cavities with a size distribution that, at least in part, overcomes nanometer dimensions.

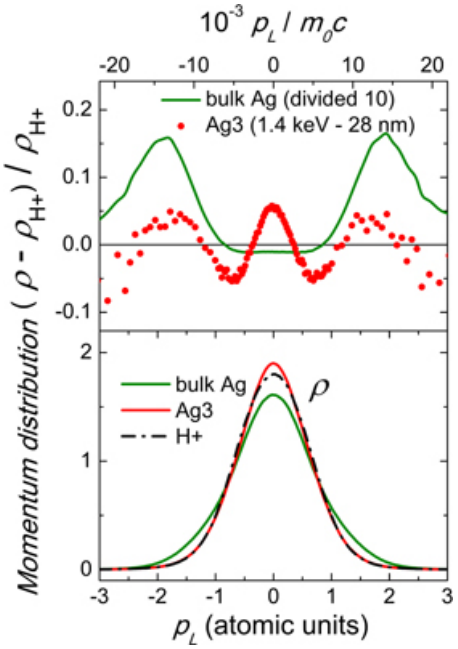


**Figure 3**. Lower panel: CDB spectra of Ag3 (1.4 keV) and H+ (1 keV). For comparison a CDB measurement of a high purity silver bulk sample (99.999% Ag) is included. Upper panel: relative difference of the momentum distributions, (ρ − ρH+)/ρH+, of the Ag3 brush and of the Ag bulk sample with respect to the protonated brush H+.

The *S*-parameter data of the upper panel of figure 2 were fitted with VEPFIT in order to estimate the layer densities (table 2). To fit PDMAEMA and H+ experimental data a three-layer model was chosen based on a brush layer, an interface and the silicon substrate. The other experimental data were fitted using a four-layer model made of a brush layer, an interlayer and the silicon substrate divided into two sections: a first layer in which an electrical field acts, and a second free from any electrical field. The use of an electric field in the four-layer model was justified because the plateaus of the S-parameter beyond the brushes layer (from 1 keV to 3 keV roughly), for all the samples except PDMAEMA, are ascribable to the presence of electric fields inside the silicon substrates: such fields drive the positrons, implanted in the silicon, towards

the interface. The value of the electric field is 2.5 ± 1.3 kV $cm^{-1}$ in the samples infiltrated with silver nanoparticles (Ag1, Ag2 and Ag3) while that for the protonated sample (H+) is lower, about 0.25 ± 0.1 kV $cm^{-1}$. The depletion region in the silicon substrate is 400 ± 100 nm for all of these samples. The electric fields are likely due to the pinning of the Fermi level at the silicon–silicon oxide interface which is composed of a native, ~1.5 nm-thick, silicon dioxide blended with the grafted alkoxysilane-type initiator layer of the same thickness and which acts as a trapping layer for positrons.

| Sample | Density (g cm−3) | Ag filling (%) | Fit variance (χ2) |
|---|---|---|---|
| PDMAEMA | 1.5 ± 0.2 | 0 | 1.73 |
| H+ | 1.5 ± 0.2 | 0 | 1.12 |
| Ag1 | 2.1 ± 0.2 | 6 ± 3 | 1.52 |
| Ag2 | 2.8 ± 0.2 | 13 ± 3 | 0.81 |
| Ag3 | 2.5 ± 0.2 | 10 ± 3 | 1.47 |

Table 2. VEPFIT results for the brush samples studied with PAS.

The calculated densities are 1.5 ± 0.2 g $cm^{-3}$ for the PDMAEMA and H+ samples while the densities for Ag1, Ag2 and Ag3 are 2.1 ± 0.2, 2.8 ± 0.2 and 2.5 ± 0.2 g $cm^{-3}$, respectively. By using a linear relation:

$$d = d_{Ag} + d_{PDMAEMA}(1 - x)$$

where $d_{Ag}$ is the Ag density (10.49 g $cm^{-3}$) and $d_{PDMAEMA}$ is the brush density (1.5 g $cm^{-3}$, according to XRR measurements), it has been possible to evaluate the percentage in mass x of the Ag nanoparticles ('Ag filling', table 2) for Ag1, Ag2 and Ag3. The values are 6 ± 3, 13 ± 3 and 10 ± 3%, respectively.

## Conclusion

We demonstrated here for the first time a completely new way to understand the structure of nanoparticle-loaded polymer brushes. Applied to pH-responsive PDMAEMA brushes, positron annihilation spectroscopy was able to discriminate between their non-protonated and the protonated forms, to give substantial information about the conformational changes experienced by the brushes after loading with silver nanoparticles and allowed one to calculate the distribution and mass concentration of the latter inside the brushes. It is worth noting that all this information was obtained by carrying out a single analysis, without making the least amount of damage to the samples. With such premises, we are sure that PAS will soon become a key technique for unlocking many of the mysteries of polymer brushes.

*Acknowledgments*

It is the authors' desire to express their greatest gratitude to Dr Laura Meda and Dr Gianluigi Marra (Eni Research Centre for Renewable Energies and Environment, Institute Eni-Donegani, Novara) for kindly providing x-ray photoelectron spectroscopy (XPS), x-ray reflectivity (XRR) measurements and electron microscopy (SEM, TEM) images.

## References

[1] Panzarasa G, Soliveri G, Sparnacci K and Ardizzone S 2015 Chem. Commun. 51 7313–6

[2] Barbey R, Lavanant L and Paripovic D 2009 Chem. Rev. 109 5437–527

[3] Chen Y and Chen J Z Y 2012 J. Polym. Sci. Part B 50 21–6

[4] Curk T, Martinez-Veracoechea F J, Frenkel D and Dobnikar J 2014 Nano Lett. 14 2617–22

[5] Kim J U and Matsen M W 2008 Macromolecules 41 246–52

[6] Milchev A, Dimitrov D I and Binder K 2008 Polymer 49 3611–8

[7] Opferman M G, Coalson R D, Jasnow D and Zilman A 2013 Langmuir 29 8584–91

[8] Kim J U and O'Shaughnessy B 2006 Macromolecules 39 413–25

[9]Liu Z, Pappacena K, Cerise J, Kim J, Durning C J, O'Shaughnessy B and Levicky R 2002 Nano Lett. 2 219–24

[10] Oren R, Liang Z, Barnard J S, Warren S C, Wiesner U and Huck W T S 2009 J. Am. Chem. Soc. 131 1670–1

[11] Dunderdale G, Howse J and Fairclough J 2011 Langmuir 27 11801–5

[12] Luzinov I, Minko S and Tsukruk V V 2008 Soft Matter 4 714–25

[13] Krishnamoorthy M and Hakobyan S 2014 Chem. Rev. 114 10976–1026

[14] Hadjesfandiari N, Yu K, Mei Y and Kizhakkedathu J N 2014 J. Mater. Chem. B 2 4968–78

[15] Gunkel G, Weinhart M, Becherer T, Haag R and Huck W T S 2011 Biomacromolecules 12 4169–72

[16] Yu Q, Shivapooja P, Johnson L M, Tizazu G, Leggett G J and López G P 2013 Nanoscale 5 3632–7

[17] Ayres N 2010 Polym. Chem. 1 769–77

[18] Moroni L, Klein M and Benetti E M 2014 Acta Biomater. 10 2367–78

[19] Ionov L, Houbenov N, Sidorenko A, Stamm M and Minko S 2006 Adv. Funct. Mater. 16 1153–60

[20] Snaith H J, Whiting G L, Sun B, Greenham N C, Huck W T S and Friend R H 2005 Nano Lett. 5 1653–7

[21] Lu Y, Liu G L and Lee L P 2005 Nano Lett. 5 5–9

[22] Tokareva I, Minko S, Fendler J H and Hutter E 2004 J. Am. Chem. Soc. 126 15950–1

[23] Roiter Y, Minko I, Nykypanchuk D, Tokarev I and Minko S 2012 Nanoscale 4 284–92

[24] Bhat R R, Tomlinson M R and Genzer J 2004 Macromol. Rapid Commun. 25 270–4

[25] Christau S, Yenice Z and Genzer J 2014 Langmuir 30 13033–41

[26] Gupta S, Uhlmann P, Agrawal M, Chapuis S, Oertel U and Stamm M 2008 Macromolecules 41 2874–9

[27] Gupta S, Agrawal M, Uhlmann P, Simon F, Oertel U and Stamm M 2008 Macromolecules 41 8152–8

[28] Fujioka T, Oshima N, Suzuki R, Price W E and Nghiem L D 2015 J. Membr. Sci. 486 106–18

[29] Kim S H, Kwak S Y and Suzuki T 2005 Environ. Sci. Technol. 39 1764–70

[30] Cano-Odena A, Vandezande P, Hendrix K, Zaman R, Mostafa K, Egger W, Sperr P, De Baerdemaeker J and Vankelecom I F J 2009 J. Phys. Chem. B 113 10170–6

[31] Nagel C, Günther-Schade K, Fritsch D, Strunskus T and Faupel F 2002 Macromolecules 35 2071–7

[32] Liao K S, Chen H, Awad S, Yuan J P, Hung W S, Lee K R, Lai J Y, Hu C C and Jean Y C 2011 Macromolecules 44 6818–26

[33] Hung W S, De Guzman M, Huang S H, Lee K R, Jean Y C and Lai J Y 2010 Macromolecules 43 6127–34

[34] Coleman P G 2003 Principles and Applications of Positron And Positronium Chemistry ed Y C Jean, P E Mallon and D M Schrader (Singapore: World Scientific) pp 37–72

[35] Rubloff G W 1990 J. Vac. Sci. Technol. A 8 1857–63

[36] Yu X et al 2015 PNAS 112 3217–22

[37] Gidley D W, Peng H G and Vallery R S 2006 Annu. Rev. Mater. Res. 36 49–79

[38] Consolati G, Ferragut R, Galarneau A, Di Renzo F and Quasso F 2013 Chem. Soc. Rev. 42 3821−3832

[39] Soles C L, Douglas J F, Wu W L, Peng H and Gidley D W 2004 Macromolecules 37 2890–900

[40] Ohrt C, Rätzke K, Oshima N, Kobayashi Y, O'Rourke B E, Suzuki R, Uedono A and Faupel F 2015 Macromolecules 48 1493–8

[41] Christau S, Thurandt S, Yenice Z and von Klitzing R 2014 Polymers 6 1877–96

[42] Chen J K, Pai P C, Chang J Y and Fan S K 2012 ACS Appl. Mater. Interfaces 4 1935–47

[43] Jones D M, Brown A and Huck W T S 2002 Langmuir 18 1265–9

[44] van der Houwen O A G J, Underberg W J M and Hennink W E 1998 Macromolecules 31 8063–8

[45] Soliveri G, Pifferi V, Panzarasa G, Ardizzone S, Cappelletti G, Meroni D, Sparnacci K and Falciola L 2015 Analyst 140 1486–94

[46] Panzarasa G 2014 J. Chem. Educ. 91 696–700

[47] van Veen A, Schut H, de Vries J, Hakvoort R A and Upma M R 1990 AIP Conf. Proc. 218 171–96

[48] Süvegh K, Domján A, Vankó G, Iván B and Vértes A 1998 Macromolecules 31 7770–5

[49] Mohsen M, Maziad N A, Gomaa E, Hassan Aly E and Mohammed R 2015 Open J. Organic Polymer Materials 5 43–52

[50] Yang J, Zhu B, Zha W, Lee M L J, Chen H and Jean Y C 2008 AIChE Annual Meeting, Conf. Proc. pp 16–21

[51] Ferragut R 2012 Physica B 407 2676–83

[52] Brusa R S, Deng W, Karwasz G P and Zecca A 2002 Nucl. Instrum. Methods Phys. Res. B 194 519–31

[53] Folegati P, Makkonen I, Ferragut R and Puska M J 2007 Phys. Rev. B 75 054201